Supplementary Information for
Entropy partitioning reveals an organization–adaptability window in open flow networks

Data and code are available to editors and reviewers upon request and will be deposited in a public repository upon acceptance.

Gérard MERLIN; Julien RAMOUSSE

LOCIE, Université Savoie Mont Blanc, CNRS, UMR5271, F-73376 Le Bourget du Lac, France

Theoretical Foundation of the Entropic Framework

Multinomial counting and Stirling expansion

Concerning multinomial counting and Stirling expansion, for N indistinguishable items allocated to M classes ($n_1 \ldots n_M$) with $\Sigma\, n_i = N$, the number of microstates (microscopic arrangements) corresponding to the number of arrangements possible by permutation and repetition is: $\Omega = \frac{N!}{\prod_i n_i!}$.

Setting $p_i = n_i / N$ with $\Sigma\, p_i = 1$ and applying Stirling-Binet's expansion for factorials, $\ln n! \approx n \ln n - n + \tfrac{1}{2} \ln(2\pi n) + O(1/n)$ gives (Appendix 1):

$$ln\Omega = -N \sum_i p_i \, ln \, p_i + \frac{1}{2}[ln(2\pi N) - \sum_i ln\,(2\pi n_i)] + \; O\left(1/N\right) \qquad \text{(S1)}$$

The expansion is asymptotically exact when every $n_i \gg 1$.

For macroscopic systems the first term dominates. However, Stirling's approximation becomes non-exact for small occupancies: retaining higher-order terms improves accuracy marginally but introduces non-extensivity (58). The remainder term $O(1/N)$ collects the next Stirling–Binet corrections, dominated by $1/(12N) - \sum_i 1/(12\, n_i)$. This notation is valid when the number of classes M is fixed and all occupancies scale with N, i.e. $n_i = N p_i$ with $p_i > 0$. If some n_i remain small, this asymptotic remainder is no longer uniformly negligible and the explicit $1/(12 n_i)$ corrections should be retained or the distribution should be coarse-grained (12). In practice, the thermodynamic limit assumption ($n_i \gg 1$) underpinning the Boltzmann–Shannon identification should be verified for small ecological networks.

Dividing $ln\ \Omega$ by $N\, k_B$ yields $\frac{S}{(N\ kB)} = \; -\Sigma\, p_i \ln p_i \equiv \; H(p)$. The half-log term grows only logarithmically with N whereas $H(p)$ grows linearly; after normalization by N it vanishes in the thermodynamic limit. Hence Boltzmann–Gibbs–Shannon entropy is precisely the leading Stirling term (11).

The usual expressions are the first dominant term (truncated series); the corrections cancel out or become negligible after normalization, explaining why these measures converge and share common properties (non-negativity, convexity, etc.).

The statistical view of missing information enables the derivation of a minimum energetic cost for logically irreversible operations such as bit erasure, formalized by Landauer's principle (59). Even for a single bit (N = 1, M = 2) the dominant entropy $k_B \ln 2$ captures the relevant physics because the residual $\tfrac{1}{2} \ln(2\pi)$ term does not scale with temperature. For an

equiprobable two-state system ($p_1 = p_2 = ½$) the Shannon entropy is $H = -\Sigma\, p_i\, log_2\, p_i = 1\ bit$ ($\equiv \ln 2\ nats$). The associated thermodynamic entropy is therefore: $S_{1bit} = k_B\, ln\, 2 \approx 9.57 \times 10^{-24}\, J\, K^{-1}$. Conversely, 1 J K^{-1} corresponds to $(1/(k_B\, ln\, 2) \approx 1.045 \times 10^{23}$ bits.

Erasing a bit compresses state space from two equiprobable states (½,½) to a single state (1,0). Bennett's theorem on reversible computation shows that only logically irreversible operations require such entropy generation (60). Hence at least $E_{min} = k_B\, T\, ln\, 2$ of heat must be dissipated. At T ≈ 300 K this is ≈ 2.9 × 10^{-21} J (≈ 18 meV). Experiments by Bérut et al. (61) confirmed the bound by measuring a dissipation close to $k_B\, T\, ln\, 2$ when erasing one bit in a colloidal particle.

Microscopic–macroscopic bridge: from local entropy production to network indicators

Each observed flow F_i aggregates a huge number of microscopic events. Defining normalized flow frequencies $p_i = F_i/F_T$ over internal, external and dissipative links allows us to evaluate Shannon entropies (for internal vs external interactions). Throughout, Shannon entropies are employed as information-theoretic functionals of normalized distribution functions (e.g., internal, boundary, and dissipative flows). It is essential to distinguish these information measures from thermodynamic entropy S, which is a state function rigorously defined only for equilibrium macrostates. Boltzmann's H-function, an information measure of the velocity distribution $f(v,t)$, is a dynamic quantity that decreases over time and should not be conflated with the equilibrium entropy S. The connection between these domains is established via statistical mechanics: thermodynamic entropy can be interpreted as the maximized Shannon entropy (or Gibbs entropy, $S = -k_B \int \rho \ln \rho\, d\Gamma$) of the full phase-space distribution (positions and momenta), evaluated in the limit of equilibrium (22) ($t \to \infty$).

In continuum nonequilibrium thermodynamics, the entropy balance at a local scale read (4-6):

$$\frac{\partial s}{\partial t} + \nabla \cdot \vec{j}_s = \sigma \geq 0 \qquad \text{(S2)}$$

Where $s(\mathrm{x}, t)$ is the specific entropy density, j_s the entropy flux (carried by heat and matter), and $\sigma(\mathrm{x}, t)$the local entropy production rate per unit volume. The latter can be decomposed into a sum of contributions from the various irreversible processes taking place in the system: heat transfer, mass diffusion, viscous dissipation, chemical reactions, charge transport, etc. Each contribution can be written in a unified force–flux form $\sigma_r = J_r X_r$, where X_r is a thermodynamic force (gradient of an intensive potential) and J_r the associated flux. Near equilibrium, the Onsager–Casimir relations linearly relate forces and fluxes, $J_r = \sum_s L_{rs}\, X_s$, with symmetric phenomenological coefficients L_{rs} (62).

Integrating the local balance over the system volume V yields the global entropy rate:

$$\frac{dS}{dt} = \int_V \sigma\, dV - \int_{\partial V} \vec{j}_s \cdot \vec{n} dA \qquad \text{(S3)}$$

which separates the internal entropy production

$$\dot{S}_{\mathrm{int}} = \int_V \sigma\, dV \qquad \text{(S4)}$$

from the entropy flux exchanged with the environment

$$\dot{S}_{\text{exch}} = \int_{\partial V} \vec{J}_s \cdot \vec{n} dA \quad \text{(S5)}$$

Where $\int_{\partial V} \vec{J}_s \cdot \vec{n} dA$ denotes the entropy flux across the system boundary, with $\vec{n}$ the outward unit normal to the surface ∂V.
In stationary systems, internal structure is maintained by exporting the entropy continuously produced inside:

$$\frac{dS}{dt} \approx 0 \Rightarrow \dot{S}_{\text{prod,int}} \approx \dot{S}_{\text{exch}}. \quad \text{(S6)}$$

In living and ecological systems, entropy production is strongly heterogeneous in space and process: some regions behave as highly dissipative transfer zones with large entropy production (e.g. turbulent transport, rapid biochemical reactions), whereas others operate as more ordered metabolic or regulatory zones, where finely tuned processes maintain local organization (4, 25). Land-surface entropy budgets show that far-from-equilibrium forcing generates spatial and temporal heterogeneity in entropy production (63). Complementary ecosystem studies further indicate that vegetation structure, successional stage and drought stress modulate radiative dissipation, exergy capture and self-organization (64). This complementarity between high-σ and low-σ subdomains may contribute to system-level robustness by distributing irreversible losses while preserving localized functional order.
At the microscopic level, thermodynamic entropy is given by Boltzmann's formula. Considering *N* indistinguishable particles distributed over M classes with occupancies $\{n_i\}$ and $p_i = n_i/N$, the multinomial multiplicity combined with the Stirling–Binet expansion leads, in the thermodynamic limit $n_i \gg 1$, to the Shannon entropy.

Mathematical development of the proposed measures

The Max-Min Entropy trade-off method combines two fundamental principles to evaluate the organization and robustness or resilience of a system:

- Maximization of external exchanges to ensure sufficient energy flow with the environment.
- Minimization of internal dissipation to guarantee maximum energy efficiency.

The system is represented as a network of nodes (compartments, objects, components, …) and connections between them.
Data are organized in input (import), output (export), dissipation vectors and in a squared matrix wherein the fluxes between nodes are reported (ENA convention).

a. External and internal entropy (H_{ext}, H_{int}) and MaxEnt reference states (support-aware)

External entropy (H_{ext}) quantifies the uncertainty (disorder) in the system's exchanges with its environment, while internal entropy (H_{int}) quantifies the uncertainty in transfers among internal nodes.
For a discrete distribution $p = (p_1 \ldots p_M)$ defined over M flow categories ("classes"), Shannon entropy is:

$$H_{ext} \text{ or } H_{int} = -\sum_{k=1}^{M} p_k \log_2(p_k), with \sum_{k=1}^{M} p_k = 1 \quad \text{(S7)}$$

Where:

$$p_k = \frac{F_k}{FT} = \frac{F_k}{\sum_{l=1}^{M} F_l}, k = 1, \dots, M \quad \text{(S8)}$$

is the probability associated with the non-zero external or internal flows (F_k).

Maximum-entropy (MaxEnt) reference states (two supports):

The interpretation of organization requires specifying a maximum-entropy (MaxEnt) reference. In network space, the key distinction lies in the support the set of links or categories over which the flow distribution is allowed to vary. A reference defined only on observed (non-zero) flows measures organization within the realized topology, whereas a reference defined on all possible flows (including structural zeros) captures the informational contribution of missing links. We therefore use two complementary MaxEnt baselines:

1. Active-link MaxEnt reference (conditioned on observed topology)

Let $\mathcal{S}_{\text{act}}$ be the set of active (non-zero) flow categories. For internal transfers, $\mathcal{S}_{\text{act,int}} = \{(i,j): F_{ij}^{\text{int}} > 0\}$ and $N_{\text{int}} = \mid \mathcal{S}_{\text{act,int}} \mid$. Similarly, $N_{\text{ext}} = \mid \mathcal{S}_{act,ext} \mid$ with $\mathcal{S}_{act,ext} = \{(i): F_i^{ext} > 0\}$ denotes the number of non-zero boundary categories considered. The MaxEnt distribution conditioned on the active support is uniform:

$$p_k^{\text{act}} = \frac{1}{M}(k \in \mathcal{S}_{\text{act}}) \quad \text{(S9)}$$

With $M = N_{int}$ or $M = N_{ext}$ for the internal and external flows, respectively, yielding: $H_{\text{max,ext}}^{\text{act}} = \log_2 N_{\text{ext}}$, $H_{\text{max,int}}^{\text{act}} = \log_2 N_{\text{int}}$.

This baseline measures organization within the realized (active) subgraph, but it does not account for structural sparsity because absent links are excluded from the support by construction.

2. Full-support maximum-entropy reference (total structural potential)

To incorporate the system's structural potential and the information carried by structural zeros (i.e., missing arcs that are topologically possible but have zero flow, as opposed to zeros arising from finite sampling or incomplete data (23), we also define a MaxEnt baseline on the full admissible support S_{full}. For an N-compartment network, the full internal potential corresponds to all N^2 donor–recipient pairs, giving the uniform baseline:

$$p_{ij}^{full} = \frac{1}{N^2}, i, j = 1, \dots, N. \quad \text{(S10)}$$

This yields the maximum internal entropy under the full-support MaxEnt reference:

$$H_{max,int}^{full} = -\sum_{i,j} \frac{1}{N^2} log_2 \left(\frac{1}{N^2}\right) = log_2(N^2) = 2log_2 N \quad \text{(S11)}$$

For boundary coupling uniformly distributed over Ncompartments: $H_{max,ext}^{full} = log_2 N$.

These full-support references are MaxEnt null models in network space and should not be conflated with microscopic thermodynamic equilibrium states in phase space.

If the realized internal network is dense ($N_{\text{int}} \approx N^2$), then $\log_2 N_{\text{int}} \approx 2\log_2 N$ and the two MaxEnt baselines converge. If the network is sparse ($N_{\text{int}} \ll N^2$), then $\log_2 N_{\text{int}} \ll 2\log_2 N$. The gap:

$$H_{\text{max,int}}^{\text{full}} - H_{\text{max,int}}^{\text{act}} = 2\log_2 N - \log_2 N_{\text{int}} = \log_2 \left(\frac{N^2}{N_{\text{int}}}\right) \quad \text{(S12)}$$

quantifies the informational contribution of structural zeros (selective connectivity), a hallmark of evolved functional networks compared with uniformly random graphs.

b. Degree of organization (α)

The degree of organization combines external and internal entropies to capture the thermodynamic trade-off between openness to the environment and internal order. Organization in far-from-equilibrium systems requires simultaneously:

-Maximizing external entropy ($H_{ext} \rightarrow H_{\max,ext}$): ensuring sufficient diversity of exchanges with the environment to sustain dissipation.

-Minimizing internal entropy ($H_{\text{int}} \rightarrow 0$): maintaining ordered internal structure to perform coherent functions.

However, a simple difference (H_{ext}- H_{int}) can yield values outside [0,1] and depends on arbitrary scaling. We therefore construct dimensionless ratios that naturally bound $\alpha \in [0,1]$.

Standard formulation (active-link reference):

$$\alpha_{ratio} = \frac{H_{ext}/H_{\max,ext}}{H_{ext}/H_{\max,ext} + H_{int}/H_{\max,int}} = \frac{H_{ext} \cdot H_{\max,int}}{H_{ext} \cdot H_{\max,int} + H_{\max,ext} \cdot H_{int}} \quad \text{(S13)}$$

where:

H_{ext}: observed external entropy

H_{int}: observed internal entropy

$H_{max,int} = log_2 N_{int}$: maximum entropy overactive internal links

$H_{max,ext} = log_2 N_{ext}$: maximum entropy overactive external flows

This ratio measures order vs. realized topology and increases when external entropy is high (diverse exchanges with environment) or when internal entropy is low (ordered internal structure). It is possible to compare systems of similar density.

At α_{ratio} = 0: system is isolated (H_{ext} = 0) or completely disordered internally ($H_{int} \rightarrow H_{\max,int}$).

At α_{ratio} = 1: system achieves maximum external openness with zero internal disorder (theoretical limit).

MaxEnt reference formulation (total potential):

Using the MaxEnt reference that accounts for all N^2 possible internal flows defined by:

$$\alpha_{ratio}^{full} = \frac{H_{ext} \cdot H_{max,int}^{full}}{H_{ext} \cdot H_{max,int}^{full} + H_{\max,ext} \cdot H_{int}} \quad \text{(S14)}$$

Where $H_{max,int}^{full} = 2log_2 N$ accounts for the complete $N \times N$ structural potential. This ratio measures order vs. total potential and is useful for cross-scale comparisons and for detecting sparsity. The gap $\Delta\alpha = \alpha_{ratio}^{full} - \alpha_{ratio}$ reflects network structural sparsity: larger gaps indicate more selective connectivity patterns characteristic of evolved networks.

c. Net external balance entropy (H_{ext2})

The external entropy (H_{ext}) treats all external flows symmetrically:

$$H_{ext} = -\sum_i p_i \log_2 p_i \qquad \text{with } p_i = \frac{F_i^{ext}}{\sum_j F_j^{ext}} \quad \text{(S15)}$$

Where $F_i^{ext} = = F_i^{in} + F_i^{out} + F_i^{diss}$

However, this formulation obscures a critical thermodynamic property: the net balance of each compartment. A mature ecosystem or sustainable system maintains approximate mass/energy balance at each node, whereas growing or declining compartments exhibit significant net accumulation or depletion.

Net balance formulation:

For each compartment *i*, we define the net balance: $F_i^{balance} = F_i^{in} - \left(F_i^{out} + F_i^{diss}\right)$. This quantity is positive for accumulating compartments (growth, storage) and negative for depleting compartments (consumption exceeds supply).

The net balance entropy is calculated from the distribution of absolute imbalances:

$$H_{ext2} = -\sum_i p_{i,2} \log_2 p_{i,2} \tag{S16}$$

Where: $p_{i,2} = \frac{|F_i^{balance}|}{\sum_j |F_i^{balance}|}$ with $\sum_i p_{i,2} = 1$.

The maximum reference assumes uniform distribution of imbalances across all *N* compartments: $H_{max,ext2} = \log_2 N$.

The following physical interpretations can then be made:

-High H_{ext2} (approaching $\log_2 N$): Imbalances are distributed across many compartments. This is characteristic of dynamic homeostasis in mature ecosystems, and the system stress is diffused rather than localized.

-Low H_{ext2} ($\ll \log_2 N$): Imbalances are concentrated in few compartments. This indicates localized dysfunction or growth hotspots, and the system may be approaching tipping point or undergoing structural transition.

-Zero H_{ext2}: Perfect balance at all compartments $\forall i\ F_i^{balance} = 0$. This theoretical steady-state is rarely observed in real systems because far-from-equilibrium, systems must maintain their organization by exporting entropy while balancing local accumulation and depletion.

The degree of organization with net balance is defined by:

$$\alpha_{ratio}^{full,2} = \frac{H_{ext2} \cdot H_{max,int}^{full}}{H_{ext2} \cdot H_{max,int}^{full} + H_{max,ext2} \cdot H_{int}} \tag{S17}$$

This formulation emphasizes the balance between:

-Distributed external imbalances (high H_{ext2}) where the system manages stress collectively.

-Ordered internal structure (low H_{int}) with efficient flow organization.

-Structural potential ($H_{max,int}^{full} = 2log_2 N$) with a capacity for complexity.

d. Dissipation penalty and effective external entropy

In the formulations α_{ratio}, α_{ratio}^{full}, and $\alpha_{ratio}^{full,2}$, dissipation is included in external entropy. However, dissipation represents degraded energy that, unlike imports and exports, does not contribute to maintaining far-from-equilibrium organization, it is the thermodynamic cost of that organization. Including dissipation equally with functional exchanges (imports/exports) can bias the inferred degree of organization, particularly in systems with high but unproductive dissipation. Across ecological datasets and, more broadly, across complex systems, “dissipative flows” are not uniquely defined: they most often correspond to respiration, but may also include non-assimilated losses, exports/rejects, or, in techno-

economic systems, dissipated heat and other losses. For this reason, we do not interpret these flows as a direct measurement of exergy gradients or of physical thermodynamic forces (i.e., gradients of intensive potentials). We adopt a mesoscopic network/information reading: "dissipation" denotes a set of flows associated with a loss of functional availability for the internal dynamics and its role is assessed through the structure of flow distributions.
We therefore introduce an effective external entropy that penalizes the dissipative contribution:
For "standard" external entropy:

$$H_{ext}^{eff} = H_{ext} - \lambda H_{diss} \tag{S18}$$

For net balance entropy:
The effective boundary-balance entropy is defined as:

$$H_{\text{bal}}^{\text{eff}} = [\, H_{bal} - \lambda \times H_{diss}]_{+} \tag{S19}$$

With: $[x]_{+} = \max(x, 0)$
Here, $H_{bal}$is the Shannon entropy of the normalized distribution of absolute node-wise boundary imbalances, and H_{diss} is the entropy of dissipative outflows. The positive-part operator $[x]_{+}$ does not introduce an additional fitted parameter; it only enforces the admissible non-negative domain of an entropy contribution. $\lambda \times H_{diss} \geq H_{bal}$, dissipative losses fully offset the effective boundary-balance contribution, so that $H_{\text{bal}}^{\text{eff}}$ is set to zero rather than allowed to become negative.

The penalized degree of organization α_{TO} becomes:

$$\alpha_{TO} = \alpha_{ratio,diss}^{full,2} = \frac{H_{ext2}^{eff} \cdot H_{max,int}^{full}}{H_{ext2}^{eff} \cdot H_{max,int}^{full} + H_{max,ext2} \cdot H_{int}} \tag{S20}$$

Determining the penalty coefficient λ: The coefficient λ should adapt to the quality of dissipation rather than being fixed at unity, because dissipation can be functionally organized in far-from-equilibrium systems (6, 25, 24). We estimate λ through three complementary hypotheses:

1. Structural component (λ_{struct}): How dispersed dissipative fluxes are across nodes:

$$\lambda_{struct} = \frac{H_{diss}}{H_{max,diss}} = \frac{H_{diss}}{\log_2 N_{diss}} \tag{S21}$$

Where $N_{diss}$is the number of compartments with non-zero dissipation.
$\lambda_{struct} \rightarrow 1$: dissipation uniformly distributed (high entropy).
$\lambda_{struct} \rightarrow 0$: dissipation concentrated (low entropy, potentially functional).

2. Thermodynamic component (λ_{thermo}): Distance from equilibrium: $\lambda_{thermo} = \frac{F_{diss}}{F_{total}}$
Where F_{diss} is total dissipation and F_{total} is total system throughput.
Low ratio: system far from equilibrium, dissipation is necessary for self-organization.
High ratio: dissipation dominates, system approaching thermodynamic efficiency limits.

3. Informational component (λ_{info}): Alignment with network structure.
We calculate Spearman correlation between dissipation distribution and topological centrality:

$$\rho = \mathrm{corr}_{\mathrm{Spearman}}(D_i, \mathrm{centrality}_i)$$

Then define four classes for $\lambda_{info} = \begin{cases} 0.0 \; if \; \rho \geq 0.7 \\ 0.3 \; if \; 0.3 \leq \rho < 0.7 \\ 0.7 \; if \; 0.0 \leq \rho < 0.3 \\ 1 \; if \; \rho < 0 \end{cases}$

If dissipation correlates strongly with high-centrality nodes, it reflects regulatory dissipation (e.g., metabolic costs of hub species maintaining network coherence) and should not be penalized. Conversely, random or anti-correlated dissipation suggests waste and merits full penalty.

This hypothesis is supported by ecological and network literature showing that functional dissipation aligns with structural coherence (65-66).

Combined penalty: $\lambda = w_1\lambda_{struct} + w_2\lambda_{thermo} + w_3\lambda_{info}$.

With weights $w_1, w_2, w_3 \geq 0$ and $w_1 + w_2 + w_3 = 1$.

Default weights (used in this study):

Structural: $w_1 = 0.2$ (moderate role: dissipation distribution matters less than other factors)

Thermodynamic: $w_2 = 0.6$ (major role: distance from equilibrium is primary determinant).

Informational: $w_3 = 0.2$ (moderate role: structural alignment indicates regulation).

These weights can be adjusted based on system-specific knowledge or calibrated against reference datasets.

Consequently, we present both unpenalized (α_{ratio}, α_{ratio}^{full}, α_{ratio}^{full2}) and penalized ($\alpha_{ratio,diss}^{full2}$) metrics, recognizing that the optimal choice depends on the analytical context and system type.

The multiple formulations of α reflect different aspects of system organization (Table S1). The choice of formulation depends on the objective set, ranging from a simple comparison of systems of similar density to a global analysis, but also on the type of data available as the distribution of external flows.

Table S1 : Formulations of degrees of organization α and significance.

Metric	Formula	Reference State	What It Measures	When to Use
α_{ratio}	$\frac{H_{ext} \cdot H_{max,int}}{H_{ext} \cdot H_{max,int} + H_{max,ext} \cdot H_{int}}$	Active links only	Organization within realized topology	Comparing systems of similar density; baseline metric
α_{ratio}^{full}	$\frac{H_{ext} \cdot H_{max,int}^{full}}{H_{ext} \cdot H_{max,int}^{full} + H_{max,ext} \cdot H_{int}}$	Full N² potential	Organization vs. total structural capacity	Multi-scale comparisons; detecting sparsity patterns
α_{ratio}^{full2}	$\frac{H_{ext2} \cdot H_{max,int}^{full}}{H_{ext2} \cdot H_{max,int}^{full} + H_{max,ext2} \cdot H_{int}}$	Full N² + net balance	Organization with homeostatic balance	Maturity assessment; resilience analysis
α_{TO}	$\frac{H_{ext2}^{eff} \cdot H_{max,int}^{full}}{H_{ext2}^{eff} \cdot H_{max,int}^{full} + H_{max,ext2} \cdot H_{int}}$	Full N² + net balance + λ penalty	Most complete: structure + balance + efficiency	captures all organizational aspects

Emergent property : adaptability

The logistic-state framework as an adaptive-capacity model.
For α and $O_\beta(\alpha) \in [0,1]$ and $\beta > 0$:

$$O_\beta(\alpha) = \frac{\alpha^\beta}{\alpha^\beta + (1-\alpha)^\beta} \tag{S22}$$

$$A_\beta(\alpha) = \frac{1}{\beta}\frac{dO_\beta}{d\alpha} = \frac{\alpha^{\beta-1}(1-\alpha)^{\beta-1}}{(\alpha^\beta + (1-\alpha)^\beta)^2} \tag{S23}$$

At the formal level, $O_\beta(\alpha)$ can be written as a two-state Boltzmann partition function:

$$O_\beta(\alpha) = \frac{e^{\beta ln\propto}}{e^{\beta ln\propto} + e^{\beta \ln(1-\propto)}} \tag{S24}$$

Where the two competing "energy levels" are *ln α* (ordered state) and *ln(1 − α)* (disordered state), and β plays the role of an inverse temperature controlling the sharpness of the order–disorder transition. In this interpretation, adaptability $A_\beta(\alpha)$is precisely the thermodynamic susceptibility of a two-state system, the sensitivity of the organizational state to infinitesimal changes in the boundary control parameter α. This susceptibility peaks sharply at $\alpha = 0.5$, defining a natural viability window whose width is governed by β: low β (≈ 2) yields a broad basin of viable thermodynamic compromise, while higher β (≈ e) selects a narrower, more stringent core of organizational compatibility (see Appendix 2 for the full derivation). From $O_\beta(\alpha)$, the adaptability $A_\beta(\alpha)$ is derived as the normalized thermodynamic susceptibility, which peaks at $\alpha = 0.5$ and defines the viability window $A_\beta(\alpha) \geq 0.9$ (see Appendix 2). Both thresholds can be tested empirically by comparing how mature natural versus anthropized systems cluster relative to $\alpha = 0.5$.

Methods (detailed)

Definition of flow matrices and boundary vectors

Each case is represented as a weighted, directed flow network with *N* nodes. We define the internal transaction matrix $F^{\text{int}} = \{F_{ij}^{\text{int}}\}$, where $F_{ij}^{\text{int}} \geq 0$ is the flow from donor compartment i to recipient compartment j. Exchanges with the environment are represented by three boundary vectors: imports = $\{F_i^{in}\}$, exports $F^{out} = \{F_i^{out}\}$, and dissipative outflows $F^{diss} = \{F_i^{diss}\}$. All computations depend only on flow magnitudes and therefore are unit-invariant provided a consistent unit is used within each network (ENA convention).
To interface directly with information-theoretic formulations of organization, flows are converted into normalized frequencies over well-defined supports. We use (i) the internal normalized matrix $P^{\text{int}} = \frac{F^{\text{int}}}{\sum_{i,j} F_{ij}^{\text{int}}}$ (when $\sum_{i,j} F_{ij}^{\text{int}} > 0$), and (ii) the external vector $F_i^{ext} = F_i^{in} + F_i^{out} + F_i^{diss}$, normalized as $P^{\text{ext}} = \frac{F_i^{ext}}{\sum_i F_i^{ext}}$ (when $\sum_i F_i^{ext} > 0$). Dissipation is also tracked separately as $P^{\text{diss}} = F_i^{diss} / \sum_i F_i^{diss}$ (when $\sum_i D_i > 0$). In all entropy calculations, zero entries are handled by restricting sums to strictly positive supports.

Computation of degree of organization α, robustness $R(\alpha)$ and adaptability $A_\beta(\alpha)$

Ulanowicz ascendancy formulation (information–entropy ratio)

To recover the classic ENA ascendancy/capacity ratio in a form consistent with our boundary representation, we build an augmented flow matrix of size $(n+2)\times(n+2)$ by embedding internal transfers, imports, and the aggregated sink (exports + dissipation). Let $T = \sum \mathrm{BigMat}$ be the total normalized mass, and $P = \mathrm{BigMat}/T$. The capacity (Shannon entropy) is $D = -\sum_{p>0} p \log_2 p,$ and the ascendancy (mutual information form) is $A = \sum_{p>0} p \log_2(\frac{p}{p_i p_j})$, where p_i and p_j are the row/column marginals of P. The degree of organization is then $\alpha_U = A/D$. This construction follows the information-theoretic foundation of ENA/ascendancy and Shannon entropy.

For all α metrics reported in this study, we map organization to a dimensionless robustness curve using the same functional form $R(\alpha) = -e\,\alpha\ln(\alpha)$, which peaks at $\alpha = 1/e$.

Adaptability formulation

For all α metrics, we also define a dimensionless adaptability curve as the normalized susceptibility of a bounded order mapping according to equations S22 and S23 which peaks at $\alpha = 0.5$ with $A_\beta(0.5) = 1$.

Max–Min entropy ratio formulation (internal vs. external structuring)

To separate internal structuring from boundary exchange demand without conflating results with total throughput, we compute entropies on normalized internal and external supports (Shannon, base 2). Internal diversity is $H_{\mathrm{int}} = -\sum_{P_{ij}^{\mathrm{int}}>0} P_{ij}^{\mathrm{int}} \log_2 P_{ij}^{\mathrm{int}}$, and its maximum is defined using (i) an active-link reference $H_{\mathrm{int}}^{\max} = \log_2(k)$, where $k$is the number of non-zero internal links, or (ii) a full-support MaxEnt structural potential reference $H_{\mathrm{int}}^{\max,\mathrm{full}} = 2\log_2(n)$, corresponding to a fully admissible $n \times n$ internal support.

External diversity is computed from the normalized Extvector as $H_{\mathrm{ext}} = -\sum_{P_i^{\mathrm{ext}}>0} P_i^{\mathrm{ext}} \log_2 P_i^{\mathrm{ext}}, H_{\mathrm{ext}}^{\max} = \log_2(k_{\mathrm{ext}})$, where k_{ext} is the number of compartments with non-zero Ext_i.

We also compute H_{diss} on P^{diss}, and a diagnostic exchange-only entropy $H_{\mathrm{ext,exch}}$ using $Z_{\mathrm{in}} + Z_{\mathrm{out}}$ (excluding D). These Shannon forms follow standard information-theoretic treatments of diversity/evenness.

The Max–Min degree of organization α_{ratio} is then computed as a bounded ratio combining (i) an external "maximization" term based on H_{ext} and its reference, and (ii) an internal "minimization" term based on H_{int} and its reference, yielding a dimensionless $\alpha \in [0,1]$ comparable across systems. We report both the active-link and equilibrium-potential normalizations and map them to robustness using $R(\alpha)$ above.

Dissipation-penalized effective external entropy (λ weighting)

Because dissipative outflows represent thermodynamic costs that may be partly functional (regulated) rather than purely "waste-like", we also report a dissipation-penalized variant (cf. section of dissipation penalty).

The penalty coefficient $\lambda \in [0,1]$ is implemented here as a bounded composite penalty coefficient rather than as a directly measured thermodynamic constant. Specifically, $\lambda = w_s\lambda_{struct} + w_t\lambda_{thermo} + w_i\lambda_{info}$, with default weights $(w_s, w_t, w_i) = (0.2,0.6,0.2)$. The structural term λ_{struct} is the normalized Shannon entropy of the dissipation vector over compartments with non-zero dissipation, thus quantifying how spatially dispersed dissipative losses are. The thermodynamic term is, by default, $\lambda_{thermo} = \sum D/(\sum F^{int} + \sum D)$, unless explicit nonequilibrium parameters are supplied. The informational term λ_{info} is a discrete score derived from the Spearman association between nodal dissipation and a flow-centrality proxy, such that strongly aligned dissipation is penalized less than weakly aligned or anti-correlated dissipation. The resulting λ is then bounded to the interval [0 1]. We therefore interpret λ as a pragmatic, sensitivity-tested dissipation penalty coefficient. Robustness $R(\alpha)$ and adaptability $A_\beta(\alpha)$ are computed from the resulting αvalues, while α_U is retained as a λ-invariant benchmark. This design follows nonequilibrium arguments that dissipation can be organized in far-from-equilibrium systems, and that functional losses can align with network structure rather than behaving as random noise.

Null-model validation

To test whether the empirical organization of each network could be explained by boundary forcing and observed topology alone, we constructed a constrained null model for the dissipation-corrected trade-off estimator. For each case, we preserved (i) the three boundary vectors, (ii) the binary internal support defined by the observed active links, and (iii) total internal throughput. Internal flow magnitudes were then randomized over the active support by drawing positive weights from a Gamma distribution and normalizing them to unity, thereby generating a Dirichlet-distributed allocation overactive links. For each null-model realization, positive random weights were first drawn on the active internal links and normalized so that their sum equals one ($\Sigma_{i,j} w_{ij}^{null} = 1$). The randomized internal matrix was then reconstructed as:

$$F_{ij}^{null} = T_{int} \times A_{ij} \times w_{ij}^{null} \tag{S25}$$

Where A_{ij} is the active-link mask and $A_{ij} = 1$ if the empirical internal link i → j is present $A_{ij} = 0$ otherwise. Here, w_{ij}^{null} is the normalized random weight assigned to the active link i → j, and T_{int} is the empirical total internal throughput. By construction, inactive links receive no flow: $F_{ij}^{null} = 0$ when $A_{ij} = 0$ and the total internal throughput is preserved: $\Sigma_{i,j} F_{ij}^{null} = T_{int}$. Equivalently, if the active links are indexed by l = 1, …, K, the null weights w_l^{null} are drawn from a Dirichlet distribution over the K active links: $w^{null} = \left(w_1^{null}, \ldots, w_K^{null}\right) \sim Dirichlet(1, \ldots, 1)$. Each active flow is then reconstructed as:

$$F_l^{null} = T_{int} \times w_l^{null} \tag{S26}$$

Before being mapped back onto the original N × N internal flow matrix.
This procedure preserves network size, active topology, and total internal flux while destroying the empirical allocation of intensities among internal links.
For each randomized realization, we recomputed internal entropy, the net external balance entropy , the dissipation-corrected organization index , and the associated robustness and adaptability derived from the corresponding value. Boundary terms were kept fixed by construction, so the null model specifically tests whether the observed internal allocation of flow intensities contributes additional organization beyond that implied by external forcing

and network support alone. For each case, we generated an ensemble of randomized networks and summarized the null distribution by its mean, standard deviation, median, and empirical vitality fractions. The empirical network was compared with this null ensemble using one-sided exceedance probabilities, two-sided empirical p-values, and standardized effect sizes , computed separately. We further quantified whether the empirical case was closer than its null expectation to the Shannon target and to the adaptability target using case-specific distance-to-target statistics. These null-model summaries were then aggregated across cases and stratified by typology to assess whether natural ecosystems show systematically stronger deviations from constrained random expectation than urban or process-type systems.

Limitations

A related caveat concerns the thermodynamic limit assumption embedded in our use of Stirling's approximation. As shown by Warren and Pettersson (58), the Boltzmann entropy expression is exact only when the ensemble size is allowed to grow without bound. For small ecological networks ($n \leq 6$), the normalized flow frequencies p_i may correspond to small effective occupancies, potentially inflating higher-order correction terms and introducing non-extensivity. We therefore recommend interpreting H_{int} and H_{ext} values for very small networks ($n < 6$) with additional caution, particularly when comparing them to large systems ($n > 30$).

Network topology, cycling, and interaction canalization

Network structural descriptors were computed with a MATLAB routine from the internal transaction matrix and boundary vectors (imports, exports, dissipative outflows). We first derive the unweighted directed adjacency matrix A, with $A_{ij} = 1$ if $F_{ij}^{\mathrm{int}} > 0$ and $A_{ij} = 0$ otherwise. From A, we compute the number of nodes n, realized links L, link density $D_L = L/n$, and connectance $C = L/n^2$.

As a proxy for structural cyclicity, we report the spectral radius of A, i.e. the largest-magnitude eigenvalue, $\lambda_{\max} \equiv \rho(A) = \max_k \mid \lambda_k(A) \mid$, which captures the potential for feedback loops independently of flow magnitudes.

We then quantify flow-based cycling using Ecological Network Analysis (ENA) and following Finn's original formulation and subsequent ENA developments (54-57).

To help interpret cross-system variations in organization indices α using flow data only (no biomasses), we further compute a structure-only interaction canalization descriptor based on donor-oriented outflow partitions. For each donor node i, the normalized distribution of its outgoing internal transfers is $s_{ij}^{\mathrm{int}} = \frac{F_{ij}^{\mathrm{int}}}{\sum_k F_{ik}^{\mathrm{int}}}$ for $\sum_k F_{ik}^{\mathrm{int}} > 0$.

Local outgoing diversity is quantified by Shannon entropy (base 2), $H_i^{(\mathrm{out,int})} = -\sum_j s_{ij}^{\mathrm{int}} \log_2 s_{ij}^{\mathrm{int}}$, then normalized by $\log_2(d_{i,\mathrm{act}}^{(\mathrm{out,int})})$, where $d_{i,\mathrm{act}}^{(\mathrm{out,int})}$ is the number of active outgoing internal links. The node-level canalization score is defined as 0: diffuse routing; 1: strongly channeled routing, and the network-level index is computed as a throughput-weighted average:

$$C_{\mathrm{net}}^{\mathrm{int}} = \sum_i w_i \; C_i^{\mathrm{int}}, w_i = \frac{\sum_j F_{ij}^{\mathrm{int}}}{\sum_{p,q} F_{pq}^{\mathrm{int}}} \tag{S27}$$

This construction leverages the long-standing use of Shannon information to characterize diversity/evenness of interaction pathways and relate pathway choice (constraints vs. redundancy) to stability arguments (17).

Finally, to match representations in which external sinks are explicitly considered, we compute an augmented version $C_{\mathrm{net}}^{\mathrm{all}}$ by applying the same entropy-normalized canalization to each node's outflow vector $\left[F_{i1}^{\mathrm{int}}, \ldots, F_{iN}^{\mathrm{int}}, Z_{\mathrm{out},i}, D_i\right]$, and weighting by total out-throughflow T_i. The normalized Shannon form is equivalent to an evenness measure (Pielou-type), previously used in interaction networks as "interaction evenness"; here we adapt it to donor-oriented outflow partitions in ENA flow networks and distinguish internal vs. augmented (with boundary sinks) throughput-weighted canalization indices.

Statistical analysis

All statistical analyses were run in MATLAB (Statistics and Machine Learning Toolbox) using two in-house scripts. One merges case-level outputs with network descriptors into a single dataset (case × variables), applies optional $\log_{10}$ transforms for highly skewed variables, and standardizes continuous descriptors (z-scores) prior to multivariate analyses to ensure comparable weighting (67-68). To limit redundancy, near-duplicate descriptors are flagged using a high Spearman rank-correlation threshold the second script then computes pairwise (and optional partial) associations, performs PCA with explained-variance reporting and case projections in the most informative planes (67-68), and explores unsupervised structure via hierarchical clustering using Ward linkage on Euclidean distances of standardized variables. To integrate heterogeneous descriptor families (e.g., topology vs. entropy-derived indicators), a multiblock "MFA-like" framework balances block contributions before global projection (69). Regression models (user-defined responses/predictors) are fitted for inference and evaluated by k-fold cross-validation when predictive performance is reported.

To diagnose the robustness ($R(\alpha)$) and adaptability (A_β) of organization ratios α across methods (m), we summarized each estimator α_m (including Ulanowicz's relative ascendency α_U) with robust location and scale statistics: the median $\tilde{\alpha}_{i,m}$ and median absolute deviation $\mathrm{MAD}_m = \mathrm{median}(|\ \alpha_{i,m} - \tilde{\alpha}_m\ |)$. Deviation from the optimal target was quantified by the signed offset $\delta_{i,m} = \alpha_{i,m} - \alpha^*$, reported as the median bias $\tilde{\delta}_m$ and $\mathrm{MAD}(\delta_{i,m})$. We also computed the empirical frequency of cases falling within the predicted viability window $[\alpha_{\min}, \alpha_{\max}]$ and its 95% confidence interval using the Wilson binomial interval. Agreement with α_U was assessed pairwise via Bland–Altman analysis: for each method m, we formed the pairwise mean $M_{i,m} = (\alpha_{i,m} + \alpha_{U,i})/2$ and difference $\Delta_{i,m} = \alpha_{i,m} - \alpha_{U,i}$, and reported the mean difference and limits of agreement $\bar{\Delta}_m \pm 1.96\, s_{\Delta,m}$. Median biases are accompanied by 95% percentile bootstrap confidence intervals on the median ($n_{\mathrm{boot}} = 20{,}000$).

Results

Bland–Altman plot

We highlight the Bland–Altman comparison between α_U and our dissipation-corrected estimator α_{TO} because it yields the tightest agreement (smallest spread of $\alpha_{TO} - \alpha_U$) while remaining interpretable physically: accounting for dissipative losses acts as a stabilizing

correction when comparing information-based and thermodynamic normalizations (Figure S1).

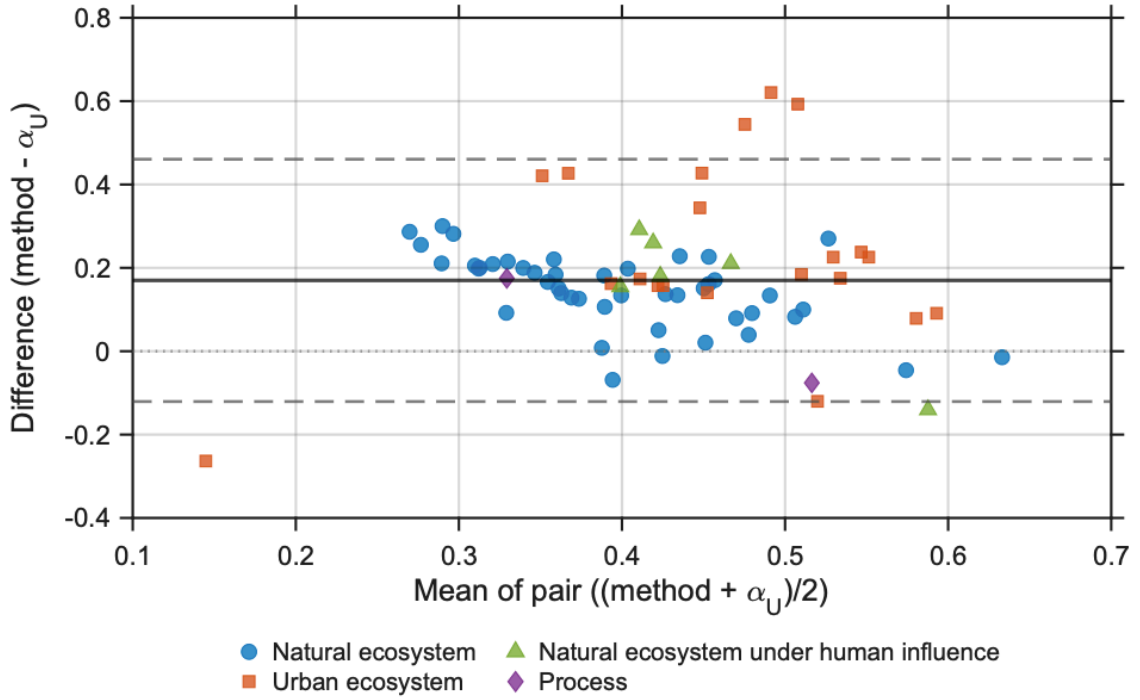

Figure S1 : Agreement between Ulanowicz's α_U and the dissipation-corrected estimator α_{TO}. Bland–Altman plot comparing α_U (Ulanowicz relative ascendency) to α_{TO} for all systems with complete data. The x-axis reports the pairwise mean $M = (\alpha_{TO} + \alpha_U)/2$; the y-axis reports the difference $\Delta = \alpha_{TO} - \alpha_U$. The solid horizontal line indicates the mean difference (bias), and dashed lines indicate the 95% limits of agreement (bias $\pm 1.96\, s_\Delta$). Systematic departures from zero and widening limits quantify method-dependent shifts and dispersion relative to Ulanowicz's formulation.

Sensitivity Analyses

Percentages refer to the proportion of cases belonging to the corresponding viability window; MWU denotes the Mann-Whitney U test.

Across the supplementary results, β acts mainly as an adaptability selectivity parameter, whereas λ acts mainly as a dissipation-penalty control parameter affecting viability-window membership.

Ulanowicz α_U did not significantly separate natural from urban systems under either kernel. By contrast, the dissipation-corrected trade-off metric produced a clear natural-urban contrast for both kernels, strongest for $\beta = 2$ (84.4% versus 38.1% in the high-A_β domain) and still significant for $\beta = e$ (64.4% versus 33.3%). This supports $\beta = 2$ as a broad baseline kernel and $\beta = e$ as a stricter sensitivity test, without changing the qualitative ecological ranking of the metrics (Table S2).

Table S2. Natural-urban contrast for adaptability under the two beta kernels

Metric	Natural median A_beta	Urban median A_beta	Natural vital proportion	Urban vital proportion	Fisher p (vitality)	MWU p (A_beta)
Ulanowicz β=2	0.686	0.748	20.0%	38.1%	0.139	0.690
Ulanowicz β=e	0.470	0.555	8.9%	19.0%	0.253	0.690
Trade-off β=2	0.957	0.843	84.4%	38.1%	3.30e-04	0.015
Trade-off β=e	0.911	0.703	64.4%	33.3%	0.033	0.015

Table note: Vital proportion corresponds to $A_\beta \geq 0.9$. Fisher p values test the difference in vitality-window membership between natural and urban systems. MWU p values compare the full A_β distributions.

The dissipation coefficient penality λ acts as a genuine control parameter for viability-window membership. At $\lambda = 0.28$, corresponding to a moderate penalty close to the empirical center of the observed values, the natural-urban contrast is simultaneously strong for robustness and adaptability, especially for A_β with $\beta = 2$. By contrast, very large penalties progressively degrade or reverse the ecological ordering, consistent with over-correction of dissipation (table S3).

Table S3. Sensitivity of the natural-urban viability contrast to the dissipation penalty lambda at representative checkpoints.

lambda	Natural p_R	Urban p_R	Fisher p (R window)	Natural p_A,beta=2	Urban p_A,beta=2	Fisher p (A_beta=2)	Natural p_A,beta=e	Urban p_A,beta=e
0.00	53.3%	28.6%	0.070	73.3%	28.6%	0.001	55.6%	28.6%
0.28	77.8%	28.6%	2.62e-04	88.9%	33.3%	8.69e-06	57.8%	28.6%
0.50	91.1%	28.6%	4.84e-07	37.8%	38.1%	1.000	31.1%	33.3%
1.00	15.6%	38.1%	0.059	8.9%	38.1%	0.013	2.2%	33.3%

Table note. p_R denotes membership in the R-based viability window; p_A, beta=2 and p_A,beta=e denote membership in the high-adaptability domains for the two kernels. Representative checkpoints were selected to illustrate no penalty, moderate penalty, strong penalty, and full penalty.

At $\beta = 0.28$, natural ecosystems cluster near the adaptability target, with high median robustness and high median adaptability under both kernels. Urban ecosystems remain shifted toward higher alpha values and lower robustness and adaptability, especially under the stricter $\beta = e$ kernel. Natural ecosystems under human influence occupy an intermediate position, whereas the process category is too small for strong inference (Table S4).

Table S4. Typology-resolved viability and median values at a representative moderate penalty (lambda = 0.28)

Group	n	p_R	p_A,beta=2	p_A,beta=e	p_joint beta=2	p_joint beta=e	median alpha	median R
Natural ecosystem	45	77.8%	88.9%	57.8%	71.1%	44.4%	0.466	0.967
Natural ecosystem under human influence	6	33.3%	83.3%	83.3%	33.3%	33.3%	0.555	0.888
Process	2	100.0%	100.0%	100.0%	100.0%	100.0%	0.505	0.936
Urban ecosystem	21	28.6%	33.3%	28.6%	28.6%	28.6%	0.620	0.806

Table note. The joint windows combine robustness and adaptability criteria. The process category contains only two cases and is shown for completeness rather than for formal inference.

Rationale for the near-optimal viability thresholds ($R \geq 0.9$ and $A_\beta \geq 0.9$)

Thermodynamic viability is assessed using two emergent, normalized properties derived from the Max–Min entropy trade-off framework: robustness $R(\alpha)$ and adaptability $A_\beta(\alpha)$. Both quantities are bounded, dimensionless functions with analytically defined optima. Viability windows are identified using the criteria $R \geq 0.9$ and $A_\beta \geq 0.9$. The rationale for these thresholds is provided below.

Both robustness and adaptability are normalized to unity at their respective theoretical maxima. A threshold of 0.9 therefore identifies configurations that retain at least 90% of the maximum achievable value of the corresponding function. Such near-optimality criteria are routinely used in physics and information-theoretic analyses to delineate stable operating regimes without requiring fine tuning. The thresholds adopted here follow directly from the mathematical structure of the functions and are not calibrated using empirical data.

Robustness threshold $R \geq 0.9$

Robustness is defined as : $R(\alpha) = -e\,\alpha\ln(\alpha)$, a parameter-free function rooted in information theory, which attains its unique maximum $R = 1$ at the Shannon-optimal value $\alpha^* = 1/e$. The condition $R \geq 0.9$ thus selects configurations lying within 10% of this theoretical maximum. This regime corresponds to a broad plateau around the optimum rather than a narrowly tuned point, thereby capturing a structurally robust domain that is resilient to moderate variations in organizational balance.

Adaptability threshold $A_\beta \geq 0.9$

Adaptability $A_\beta(\alpha)$ is defined as the normalized susceptibility of the bounded organizational state function $O_\beta(\alpha)$. Formally, it is equivalent to a thermodynamic susceptibility in a two-state Boltzmann representation and quantifies the capacity of a system to reorganize in response to changes in boundary constraints.

The function $A_\beta(\alpha)$ reaches its maximum at $\alpha^* = 0.5$, independently of the value of β. The criterion $A_\beta \geq 0.9$ therefore identifies near-critical regimes that retain at least 90% of the maximal adaptive capacity. The parameter β controls the width of this high-adaptability domain but does not affect the position of the optimum, ensuring that the threshold is not tied to a specific kernel choice.

Joint viability criterion and robustness to threshold choice

Robustness and adaptability capture complementary aspects of system viability. High robustness alone may be associated with rigid, over-organized configurations, whereas high adaptability alone may characterize weakly organized or unstable regimes. Imposing the joint criteria $R \geq 0.9$ and $A_\beta \geq 0.9$ thus delineates a near-optimal viability domain that excludes both extremes.

Sensitivity analyses reported in Supplementary Tables S2–S3 demonstrate that the main qualitative patterns identified in this study are robust to moderate variations in threshold values. This confirms that the inferred viability domain reflects a structurally stable region of the organization–entropy trade-off space rather than a finely adjusted cutoff.

In summary, the thresholds $R \geq 0.9$ and $A_\beta \geq 0.9$ operationalize a near-optimal thermodynamic viability regime grounded in the normalized structure and analytically defined optima of robustness and adaptability functions. By retaining configurations within 10% of their respective theoretical maxima, these criteria identify a broad and stable domain of viable organization without relying on arbitrary or empirically tuned thresholds.

Pareto Front

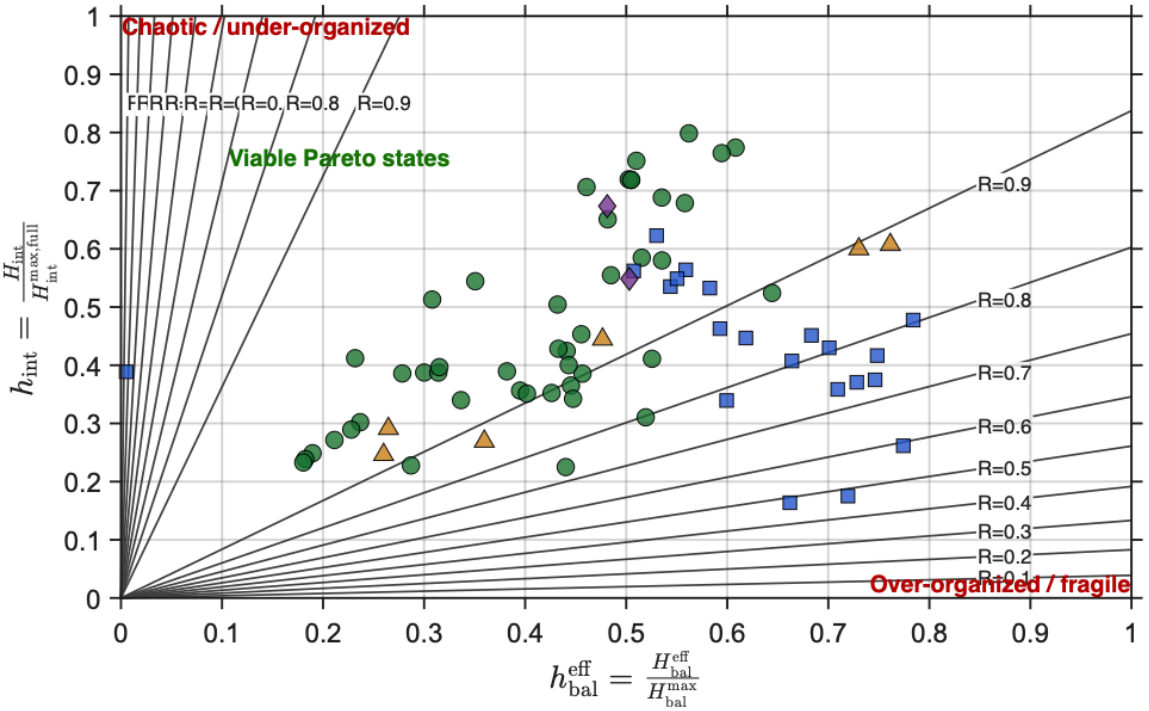

Figure S2: Entropy Trade-off Pareto Front for R according α_{TO} for β=2.

Robustness is positioned in a plane defined by normalized internal and external flows showing the iso curves of this property. In this plane, the horizontal axis represents the effective equilibrium entropy at the boundaries illustrating the diversity of the distribution of nodal disequilibria between imports, exports and dissipative losses, while the vertical axis represents the disorder of internal flows. Each point represents an empirical system and isocurves are superimposed to delimit the joint viability domain for values ≥ 0.9. The distribution of robustness of empirical systems on this plane reveals a striking asymmetry like adaptability property. Natural ecosystems cluster within or near the viability domain and

Urban systems, by contrast, are displaced away from this viability domain toward a region where boundary-exchanges diversity is insufficient relative to internal flow disorder.

Null-model validation of the entropy trade-off signal

To test whether the observed organization of empirical networks exceeded constrained random expectation, we compared each case with a null ensemble preserving boundary conditions, active topology, and total internal throughput while randomizing the allocation of internal flow intensities (Tables S4 and S5). Across the 74 cases, empirical networks showed positive global median deviations from null expectation for both organization and adaptability ($median\ z_{alpha} = 7.16$, $median\ z_A = 4.06$), whereas robustness relative to the Shannon curve was globally lower than null expectation ($median\ z_R = -3.94$). Typology significantly affected z_{alpha} (Kruskal–Wallis $p = 0.0126$), z_A ($p = 2.43\ 10^{-5}$), and proximity to the adaptability target $\alpha^* = 0.5$ ($\Delta_{target,a}$, $p = 1.94\ 10^{-5}$), but not z_R or proximity to the Shannon target 1/e. Natural ecosystems differed significantly from other systems for z_{alpha}, z_A, and $\Delta_{target,a}$, whereas no significant separation was detected for z_R or $\Delta_{target,e}$. Median deviations above null expectation were much larger in natural ecosystems ($med\ z_{alpha} = 36.08$, $med\ z_A = 8.70$) than in urban ecosystems ($med\ z_{alpha} = 3.42$, $med\ z_A = -1.82$). These results show that the null-model signal is primarily expressed through elevated organization and adaptive positioning around $\alpha^* = 0.5$, rather than through a closer approach to the Shannon robustness optimum.

Table S4. *Null-model validation summary by typology.* Median deviations from null expectation for organization (z_{alpha}), adaptability (z_A), robustness (z_R), and distance to the Shannon ($\Delta Sh = {}^{1}/_{e}$) and adaptability ($\Delta A = 0.5$) targets.

Δ target (1/e) = mean null distance to 1/e minus empirical distance; positive values indicate that the empirical network is closer to the Shannon target than its null expectation. Δ target (0.5) is defined analogously for the adaptability target α=0.5.*

System class	n	Median z_alpha	Median z_A	Median z_R	Median Δ target (1/e)	Median Δ target (0.5)	Prop. p_alpha<0.05	Prop. p_A<0.05	Prop. better than null vs 0.5
Natural ecosystem	46	36.0779	8.7031	-4.5341	-0.0175	0.0386	0.933	0.867	0.933
Natural ecosystem under human influence	5	2.2248	1.3360	0.6116	-0.0087	0.0390	0.600	0.400	1.000
Process	2	2.9860	3.6155	-3.5324	0.0175	0.0107	0.500	0.500	1.000
Urban ecosystem	21	3.4247	-1.8236	-3.2208	-0.0425	-0.0263	0.762	0.238	0.286

685
686 **Table S5.** *Case-level null-model statistics.* Empirical values, null-model deviations, target-distance statistics, empirical exceedance probabilities,
687 and retained randomization counts for all classified cases.

Cases are ordered by system class and case name. One unmatched case name ('CAP-N-Land') was excluded from this table because no typology could be assigned automatically.

Case	System class	alpha_emp	R_emp	A_emp	z_alpha	z_A	z_R	Δ target (1/e)	Δ target (0.5)	p_alpha_ge	p_A_ge	p_R_ge	K_valid
Baie de Somme	Natural ecosystem	0.5013	0.9410	1.0000	8.9583	4.8401	-14.1667	-0.0822	0.0797	0.000	0.000	1.000	1000
Baltic Sea	Natural ecosystem	0.3917	0.9979	0.8697	3.8213	3.6578	-7.6822	-0.0191	0.0233	0.003	0.003	0.997	1000
Benguela	Natural ecosystem	0.4253	0.9884	0.9355	9.3536	8.7031	-10.9591	-0.0160	0.0160	0.000	0.000	1.000	1000
Biscay	Natural ecosystem	0.4400	0.9819	0.9579	4.2217	4.1100	-4.3286	-0.0042	0.0042	0.000	0.000	1.000	1000
CHBay_1950	Natural ecosystem	0.4393	0.9823	0.9568	67.4426	57.3199	8.6753	0.0202	0.1630	0.000	0.000	0.000	1000
CHBay_1960	Natural ecosystem	0.4406	0.9817	0.9586	71.0886	61.0126	10.5536	0.0263	0.1716	0.000	0.000	0.000	1000
CHBay_1970	Natural ecosystem	0.4376	0.9831	0.9544	77.4914	68.9615	15.4846	0.0440	0.1834	0.000	0.000	0.000	1000
CHBay_1980	Natural ecosystem	0.4325	0.9854	0.9469	89.9310	84.5469	22.7071	0.0690	0.1982	0.000	0.000	0.000	1000
CHBay_1990	Natural ecosystem	0.4333	0.9851	0.9481	94.5504	90.1591	24.5229	0.0750	0.2058	0.000	0.000	0.000	1000
CHBay_2000	Natural ecosystem	0.4365	0.9836	0.9529	96.0795	91.4259	24.2350	0.0737	0.2110	0.000	0.000	0.000	1000
Chesapeake_Bay	Natural ecosystem	0.5255	0.9191	0.9923	40.2418	14.3361	-74.9187	-0.1055	0.0546	0.000	0.000	1.000	1000
ConeSpring	Natural ecosystem	0.5095	0.9339	0.9989	2.2004	1.4132	-2.3034	-0.0551	0.0383	0.036	0.043	0.964	1000
CrystalRiver	Natural ecosystem	0.5575	0.8854	0.9611	76.3297	34.5237	-49.9673	-0.1204	0.1439	0.000	0.000	1.000	1000
EasternScotian	Natural ecosystem	0.4131	0.9927	0.9137	0.0401	0.0447	-0.0298	0.0000	0.0000	0.468	0.468	0.532	1000
Florida Bay (dry)	Natural ecosystem	0.5256	0.9190	0.9922	470.4273	226.6235	-1352.4082	-0.1373	0.1269	0.000	0.000	1.000	1000
Florida Bay (wet)	Natural ecosystem	0.5336	0.9111	0.9866	475.8056	210.5845	-1902.3657	-0.1497	0.1146	0.000	0.000	1.000	1000
FloridaBay	Natural ecosystem	0.4512	0.9761	0.9719	5.3694	5.0552	-5.5973	-0.0078	0.0078	0.000	0.000	1.000	1000
Gulf of Maine	Natural ecosystem	0.3751	0.9998	0.8308	82.5415	78.9332	36.1816	0.0786	0.0931	0.000	0.000	0.000	1000
GulfCorinth	Natural ecosystem	0.4369	0.9834	0.9534	2.0481	2.0264	-2.0698	-0.0022	0.0022	0.029	0.029	0.971	1000
Kromme_Estuary	Natural ecosystem	0.5494	0.8945	0.9712	47.9569	11.7050	-120.4102	-0.1420	0.0432	0.000	0.000	1.000	1000
Marion Lake	Natural ecosystem	0.5611	0.8813	0.9563	3.5053	-3.1208	-3.9913	-0.0801	-0.0353	0.006	0.994	0.994	1000
Menez_Gwen	Natural ecosystem	0.4684	0.9656	0.9881	1.4267	1.4594	-1.3789	-0.0175	0.0177	0.073	0.072	0.927	1000
MuddySand	Natural ecosystem	0.4951	0.9461	0.9997	37.0031	20.6321	-72.4589	-0.0871	0.0871	0.000	0.000	1.000	1000
NorthSea	Natural ecosystem	0.6258	0.7974	0.8285	6.2507	-12.4351	-7.5002	-0.1018	-0.1016	0.000	1.000	1.000	1000
Okefenokee Swamp	Natural ecosystem	0.4974	0.9443	0.9999	72.2506	44.2938	-72.0315	-0.0909	0.1680	0.000	0.000	1.000	1000
Olentangy	Natural ecosystem	0.6617	0.7427	0.7337	15.4455	-15.9968	-29.2577	-0.2125	-0.1110	0.000	1.000	1.000	1000
RainForest	Natural ecosystem	0.5514	0.8923	0.9688	-1.1758	0.9497	1.0545	0.0386	0.0386	0.936	0.064	0.064	1000
Reef	Natural ecosystem	0.4614	0.9701	0.9823	2.2977	2.1399	-2.3378	-0.0376	0.0378	0.025	0.024	0.975	1000
SB_1600	Natural ecosystem	0.4112	0.9933	0.9101	4.2119	4.1093	-4.5341	-0.0066	0.0066	0.000	0.000	1.000	1000
SB_1900	Natural ecosystem	0.4125	0.9929	0.9127	4.4851	4.3682	-4.8355	-0.0071	0.0071	0.000	0.000	1.000	1000
SB_1960	Natural ecosystem	0.4128	0.9928	0.9131	4.5711	4.4471	-4.9422	-0.0072	0.0072	0.000	0.000	1.000	1000
SB_1978	Natural ecosystem	0.3948	0.9974	0.8764	3.1503	3.1091	-3.4277	-0.0048	0.0048	0.003	0.003	0.997	1000
StMarks_1	Natural ecosystem	0.5026	0.9399	0.9999	47.2460	24.1567	-90.0571	-0.0908	0.0855	0.000	0.000	1.000	1000
Sundarban Mangrove (reclaimed)	Natural ecosystem	0.4800	0.9577	0.9952	3.6527	2.8981	-3.9409	-0.0222	0.0222	0.004	0.004	0.996	1000
Sundarban Mangrove (virgin)	Natural ecosystem	0.4664	0.9669	0.9866	5.6700	4.4933	-6.7628	-0.0335	0.0335	0.000	0.000	1.000	1000
Sunday_Estuary	Natural ecosystem	0.5422	0.9022	0.9789	41.2979	11.0881	-91.0482	-0.1291	0.0447	0.000	0.000	1.000	1000
Swartkops_Estuary	Natural ecosystem	0.5665	0.8751	0.9484	52.6007	8.1088	-146.5979	-0.1612	0.0282	0.000	0.000	1.000	1000
Sylt-Romo Bight (C)	Natural ecosystem	0.4427	0.9806	0.9614	80.7852	63.6321	-35.4224	-0.0377	0.1119	0.000	0.000	1.000	1000
Sylt-Romo Bight (N)	Natural ecosystem	0.3599	0.9998	0.7923	92.8534	92.3548	47.1266	0.0997	0.0997	0.000	0.000	0.000	1000
Sylt-Romo Bight (P)	Natural ecosystem	0.4191	0.9907	0.9247	106.7873	92.8455	15.9786	0.0196	0.1220	0.000	0.000	0.000	1000
nes97	Natural ecosystem	0.5474	0.8966	0.9734	36.0779	7.5093	-72.0673	-0.1267	0.0318	0.000	0.000	1.000	1000
ns_1890	Natural ecosystem	0.4364	0.9836	0.9528	100.1629	84.8693	11.6068	0.0165	0.1536	0.000	0.000	0.000	1000
ns_1974	Natural ecosystem	0.4375	0.9831	0.9543	10.9464	9.9117	-12.6606	-0.0180	0.0180	0.000	0.000	1.000	1000
ns_1990	Natural ecosystem	0.4477	0.9780	0.9678	104.5259	84.8946	2.8050	-0.0010	0.1586	0.000	0.000	0.005	1000
ns_1991	Natural ecosystem	0.4043	0.9952	0.8966	2.9948	2.9761	-3.0612	-0.0019	0.0019	0.003	0.003	0.997	1000
CAP-N-	Natural ecosystem under human influence	0.5564	0.8867	0.9627	-0.6071	0.6211	0.6116	0.0064	0.0064	0.695	0.305	0.305	1000
CAPWN	Natural ecosystem under human influence	0.5174	0.9268	0.9964	-0.7801	0.6008	0.7310	0.0249	0.0251	0.790	0.210	0.210	1000
Mdloti Estuary (C, March 2002)	Natural ecosystem under human influence	0.5719	0.8686	0.9400	215.6102	69.6174	-471.5575	-0.1720	0.0922	0.000	0.000	1.000	1000
Mondego	Natural ecosystem under human influence	0.4763	0.9603	0.9933	206.6115	159.0700	1.0425	-0.0087	0.2081	0.000	0.000	0.151	1000
Trinket	Natural ecosystem under human influence	0.5135	0.9304	0.9978	2.2248	1.3360	-2.2106	-0.0632	0.0390	0.023	0.069	0.977	1000
Aqua1	Process	0.4785	0.9588	0.9944	-1.1878	0.3838	1.0054	0.0459	0.0106	0.938	0.499	0.062	1000
SantaPola	Process	0.4168	0.9915	0.9206	7.1597	6.8472	-8.0703	-0.0109	0.0109	0.000	0.000	1.000	1000
Beijing	Urban ecosystem	0.7557	0.5754	0.4640	7.8739	-20.1590	-11.7905	-0.2616	-0.2296	0.000	1.000	1.000	1000
Beijing-1995	Urban ecosystem	0.7475	0.5914	0.4871	3.4247	-3.6702	-3.6803	-0.1213	-0.1213	0.011	0.989	0.989	1000
Beijing-2000	Urban ecosystem	0.6627	0.7412	0.7312	2.4180	-2.5978	-2.4769	-0.0777	-0.0777	0.026	0.974	0.974	1000
Beijing-2005	Urban ecosystem	0.8042	0.4763	0.3355	1.7828	-1.8180	-1.7832	-0.0939	-0.0939	0.064	0.936	0.936	1000
BeijingNP	Urban ecosystem	0.5225	0.9220	0.9940	8.6846	-0.1030	-10.0546	-0.0439	-0.0011	0.000	0.560	1.000	1000
BeijingNP-1996	Urban ecosystem	0.5040	0.9387	0.9998	8.5916	4.0567	-10.1477	-0.0425	0.0346	0.000	0.000	1.000	1000
BeijingNP-2000	Urban ecosystem	0.4978	0.9439	0.9999	5.6513	3.2269	-6.2786	-0.0295	0.0295	0.000	0.000	1.000	1000
BeijingNP-2004	Urban ecosystem	0.4978	0.9439	0.9999	5.6476	3.1853	-6.2925	-0.0292	0.0292	0.000	0.000	1.000	1000
BeijingNP-2008	Urban ecosystem	0.5008	0.9415	1.0000	7.2466	3.6975	-8.3463	-0.0361	0.0346	0.000	0.000	1.000	1000
GalveP	Urban ecosystem	0.6023	0.8301	0.8828	1.9422	-2.0219	-1.9725	-0.0253	-0.0253	0.048	0.952	0.952	1000
MD_2010_split_reconst	Urban ecosystem	0.5806	0.8581	0.9254	8.2588	-19.0669	-9.5383	-0.0639	-0.0639	0.000	1.000	1.000	1000
MD_2019_split	Urban ecosystem	0.5615	0.8809	0.9557	7.6352	-28.7414	-8.8215	-0.0580	-0.0552	0.000	1.000	1.000	1000
StockholmNP	Urban ecosystem	0.6385	0.7787	0.7965	2.8420	-3.2200	-3.0058	-0.0600	-0.0600	0.013	0.987	0.987	1000
StockholmNP-N	Urban ecosystem	0.6198	0.8060	0.8430	2.6183	-2.8113	-2.7017	-0.0343	-0.0343	0.015	0.985	0.985	1000
Suzhou	Urban ecosystem	0.0131	0.1547	0.0137	101.7414	103.8265	91.3837	0.0069	0.0069	0.000	0.000	0.000	1000
Swiss	Urban ecosystem	0.4598	0.9711	0.9808	-1.4012	-1.8236	1.2357	0.0254	-0.0200	0.965	0.955	0.035	1000
Toronto-N	Urban ecosystem	0.6642	0.7387	0.7268	0.9395	-0.9109	-0.8879	-0.0263	-0.0263	0.142	0.858	0.858	1000
Toronto-N-1990	Urban ecosystem	0.6656	0.7365	0.7230	0.5222	-0.4930	-0.4651	-0.0158	-0.0158	0.226	0.774	0.774	1000
Toronto-N-2001	Urban ecosystem	0.6424	0.7728	0.7862	-0.3148	0.3385	0.3292	0.0094	0.0094	0.562	0.438	0.438	1000
Vienna	Urban ecosystem	0.6214	0.8036	0.8392	3.0704	-3.4557	-3.2208	-0.0499	-0.0499	0.013	0.987	0.987	1000
Xiamen	Urban ecosystem	0.6198	0.8060	0.8431	4.3355	-5.8787	-4.8074	-0.0685	-0.0685	0.001	0.999	0.999	1000

688

References

1. Riva, F. et al. Toward a cohesive understanding of ecological complexity. *Sci. Adv.* **9**, eabq4207 (2023).
2. Herrmann-Pillath, C. The case for a new discipline: Technosphere science. *Ecol. Econ.* **149**, 212-225 (2018).
3. Volk, T. & Pauluis, O. It is not the entropy you produce, rather, how you produce it. *Philos. Trans. R. Soc. B Biol. Sci.* **365**, 1317-1322 (2010).
4. Prigogine, I. *Introduction to Thermodynamics of Irreversible Processes* 3rd edn (Interscience, 1967).
5. Dewar, R. C. Information theory explanation of the fluctuation theorem, maximum entropy production, and self-organized criticality in non-equilibrium stationary states. *J. Phys. A Math. Gen.* **36**, 631–641 (2003).
6. Martyushev, L. M. & Seleznev, V. D. Maximum entropy production principle in physics, chemistry and biology. *Phys. Rep.* **426**, 1–45 (2006).
7. Kleidon, A. A basic introduction to the thermodynamics of the Earth system far from equilibrium and maximum entropy production. *Philos. Trans. R. Soc. B Biol. Sci.* **365**, 1303–1315 (2010).
8. Endres, R. G. Entropy production selects nonequilibrium states in multistable systems. *Sci. Rep.* **7**, 14437 (2017).
9. Schröder, A., Persson, L. & de Roos, A. M. Direct experimental evidence for alternative stable states: a review. *Oikos* **110**, 3–19 (2005).
10. Jaynes, E. T. Information theory and statistical mechanics. *Phys. Rev.* **106**, 620–630 (1957).
11. Shannon, C. E. A mathematical theory of communication. *Bell Syst. Tech. J.* **27**, 379–423 (1948).
12. Cover, T. M. & Thomas, J. A. *Elements of Information Theory* 2nd edn (Wiley-Interscience, 2006).
13. Penrose, R. *Cycles of Time: An Extraordinary New View of the Universe* (Knopf, 2010).
14. Kay, J. J. Ecosystems as self-organizing holarchic open systems: narratives and the second law of thermodynamics. In *Handbook of Ecosystem Theories and Management* (eds Jørgensen, S. E. & Müller, F.) 135–160 (CRC Press, 2000).
15. Kleidon, A. A principle of maximum entropy production emerges from thermodynamic trade-offs. *Philos. Trans. R. Soc. A Math. Phys. Eng. Sci.* **380**, 20210075 (2022).
16. Fath, B. D. et al. Ecological network analysis metrics: the need for an entire ecosystem approach in management and policy. *Ocean Coast. Manag.* **174**, 1–14 (2019).
17. Ulanowicz, R. E. Information theory in ecology. *Comput. Chem.* **25**, 393–399 (2001).
18. Lotka, A. J. Contribution to the energetics of evolution. *Proc. Natl Acad. Sci. USA* **8**, 147–151 (1922).
19. Odum, H. T. & Pinkerton, R. C. Time's speed regulator: the optimum efficiency for maximum power output in physical and biological systems. *Am. Sci.* **43**, 331–343 (1955).

20. Odum, H. T. Maximum power and efficiency: a rebuttal. *Ecol. Model.* **20**, 71–82 (1983).
21. Chapman, E. J., Childers, D. L. & Vallino, J. J. How the second law of thermodynamics has informed ecosystem ecology through its history. *BioScience* **66**, 27–39 (2016).
22. Ben-Naim, A. Entropy, Shannon's measure of information and Boltzmann's H-theorem. *Entropy* **19**, 48 (2017).
23. Templ, M., Hron, K. & Filzmoser, P. Exploratory tools for outlier detection in compositional data with structural zeros. *J. Appl. Stat.* **44**, 734–752 (2017).
24. Prigogine, I. Time, structure, and fluctuations. *Science* **201**, 777–785 (1978).
25. Schneider, E. D. & Kay, J. J. Life as a manifestation of the second law of thermodynamics. *Math. Comput. Model.* **19**, 25–48 (1994).
26. Weaver, W. Science and complexity. *Am. Sci.* **36**, 536–544 (1948).
27. Gorban, A. N., Tyukina, T. A., Pokidysheva, L. I. & Smirnova, E. V. Dynamic and thermodynamic models of adaptation. *Phys. Life Rev.* **37**, 17–64 (2021).
28. Haegeman, B. & Loreau, M. Limitations of entropy maximization in ecology. *Oikos* **117**, 1700–1710 (2008).
29. Trancón y Widemann, B. & Bogner, C. What's flux got to do with it? Non-equilibrium thermodynamics, information and the main claims of Ulanowicz's ascendancy: a critical discussion. Preprint at https://arxiv.org/abs/1602.05056 (2016).
30. Holling, C. S. Cross-scale morphology, geometry, and dynamics of ecosystems. *Ecol. Monogr.* **62**, 447–502 (1992).
31. Gunderson, L. H. & Holling, C. S. (eds) *Panarchy: Understanding Transformations in Human and Natural Systems* (Island Press, 2002).
32. Borrett, S. R. Throughflow centrality is a global indicator of the functional importance of species in ecosystems. *Ecol. Indic.* **32**, 182–196 (2013).
33. Rosales, F. O., Fath, B. D. & Llerena, G. Y. Quantifying a virtual water metabolic network of the Metropolitan District of Quito, Ecuador, using ecological network methods. *J. Ind. Ecol.* **27**, 1304–1318 (2023).
34. Yang, R., Feng, M., Liu, Z., Wang, X. & Qu, Z. Analysis of keystone species in a quantitative network perspective based on stable isotopes. *Ecol. Complex.* **59**, 101092 (2024).
35. Feng, J. et al. Mediating role of food web structure in linking diversity to multidimensional stability: evidence from global marine ecosystems. *Sci. Adv.* **11**, eadv3841 (2025).
36. Ulanowicz, R. E. Quantitative methods for ecological network analysis. *Comput. Biol. Chem.* **28**, 321–339 (2004).
37. Higashi, M. & Patten, B. C. Dominance of indirect effects in ecosystems. *Am. Nat.* **133**, 288–302 (1989).
38. Borrett, S. R. & Salas, A. K. Indirect effects and cycling in ecological networks: a comparison of indices. *Ecol. Model.* **221**, 2908–2919 (2010).
39. Liu, G. & Wu, M. Thermodynamic-based ecological scaling theory in urban metabolic framework: a review. *Front. Environ. Sci. Eng.* **19**, 4 (2025).
40. Pelorosso, R., Gobattoni, F. & Leone, A. The low-entropy city: a thermodynamic approach to reconnect urban systems with nature. *Landsc. Urban Plan.* **168**, 22–30 (2017).

41. Bristow, D. & Kennedy, C. Why do cities grow? Insights from nonequilibrium thermodynamics at the urban and global scales. *J. Ind. Ecol.* **19**, 211–221 (2015).
42. Eppinga, M. B. et al. Long-term transients help explain regime shifts in consumer-renewable resource systems. *Commun. Earth Environ.* **2**, 42 (2021).
43. Baird, D. & Ulanowicz, R. E. The seasonal dynamics of the Chesapeake Bay ecosystem. *Ecol. Monogr.* **59**, 329–364 (1989).
44. Ryser, R., Hirt, M. R., Häussler, J., Gravel, D. & Brose, U. Landscape heterogeneity buffers biodiversity of simulated meta-food-webs under global change through rescue and drainage effects. *Nat. Commun.* **12**, 4716 (2021).
45. Wollrab, S. et al. Climate change-driven regime shifts in a planktonic food web. *Am. Nat.* **197**, 281–295 (2021).
46. Khalil, H. K. *Nonlinear Systems* 3rd edn (Prentice Hall, 2002).
47. Kullback, S. & Leibler, R. A. On information and sufficiency. *Ann. Math. Stat.* **22**, 79–86 (1951).
48. Karunanithi, A. T., Cabezas, H., Frieden, B. R. & Pawlowski, C. W. Detection and assessment of ecosystem regime shifts from Fisher information. *Ecol. Soc.* **13**, 22 (2008).
49. Chaisson, E. J. Energy rate density as a complexity metric and evolutionary driver. *Complexity* **16**, 27–40 (2011).
50. Amari, S.-I. *Information Geometry and Its Applications* (Springer, 2016).
51. Colléter, M. et al. Global overview of the applications of the Ecopath with Ecosim modeling approach using the EcoBase models repository. *Ecol. Model.* **302**, 42–53 (2015).
52. Borrett, S. R. & Lau, M. K. enaR: an R package for ecosystem network analysis. *Methods Ecol. Evol.* **5**, 1206–1213 (2014).
53. Ulanowicz, R. E. *A Third Window: Natural Life Beyond Newton and Darwin* (Templeton Foundation Press, 2009).
54. Finn, J. T. Measures of ecosystem structure and function derived from analysis of flows. *J. Theor. Biol.* **56**, 363–380 (1976).
55. Fath, B. D. & Patten, B. C. Review of the foundations of network environ analysis. *Ecosystems* **2**, 167–179 (1999).
56. Fath, B. D., Scharler, U. M., Ulanowicz, R. E. & Hannon, B. Ecological network analysis: network construction. *Ecol. Model.* **208**, 49–55 (2007).

Additional references in Supplementary Information

57. Allesina, S. & Ulanowicz, R. E. Cycling in ecological networks: Finn's index revisited. *Comput. Biol. Chem.* **28**, 227–233 (2004).
58. Warren, P. B. & Pettersson, J. R. Quirks of Stirling's approximation. *J. Chem. Educ.* **90**, 731–734 (2013).
59. Landauer, R. Irreversibility and heat generation in the computing process. *IBM J. Res. Dev.* **5**, 183–191 (1961).
60. Bennett, C. H. The thermodynamics of computation—a review. *Int. J. Theor. Phys.* **21**, 905–940 (1982).
61. Bérut, A. et al. Experimental verification of Landauer's principle linking information and thermodynamics. *Nature* **483**, 187–189 (2012).

62. Pavelka, M., Klika, V. & Grmela, M. Time reversal in nonequilibrium thermodynamics. *Phys. Rev. E* **90**, 062131 (2014).
63. Brunsell, N. A., Schymanski, S. J. & Kleidon, A. Quantifying the thermodynamic entropy budget of the land surface: is this useful? *Earth Syst. Dyn.* **2**, 87–103 (2011).
64. Song, Q. H. et al. The effect of drought stress on self-organisation in a seasonal tropical rainforest. *Ecol. Model.* **265**, 136–139 (2013).
65. Estrada, E. *The Structure of Complex Networks: Theory and Applications* (Oxford University Press, 2012).
66. Jalili, M. & Perc, M. Information cascades in complex networks. *J. Complex Netw.* **5**, 157–176 (2017).
67. Jolliffe, I. T. *Principal Component Analysis* 2nd edn (Springer, 2002).
68. Abdi, H. & Williams, L. J. Principal component analysis. *Wiley Interdiscip. Rev. Comput. Stat.* **2**, 433–459 (2010).
69. Escofier, B. & Pagès, J. Multiple factor analysis (AFMULT package). *Comput. Stat. Data Anal.* **18**, 121–140 (1994).

Appendix 1: mathematical demonstration for Stirling-Binet approximation and entropy formulas

Considering that microstates arrangements (multinomial multiplicity) is:

$$\Omega = \frac{N!}{\prod_i n_i!}$$

And with $N = \sum_i^m n_i$, by applying the logarithm:

$$ln\Omega = lnN! - \sum_{i=1}^{m} ln\, n_i!$$

Using Stirling-Binet's asymptotic expansion for each factorial:
For any large integer x_i:

$$lnx! = x\, lnx - x + \frac{1}{2}ln(2\pi x) + \frac{1}{12x} + O\left(\frac{1}{x^3}\right)$$

Gives for $N!\, and\, n_i!$:

$$lnN! = N\, lnN - N + \frac{1}{2}ln(2\pi N) + \frac{1}{12N} + O\left(\frac{1}{N^3}\right)$$

$$ln\, n_i! = n_i\, ln\, n_i - n_i + \frac{1}{2}ln(2\pi n_i) + \frac{1}{12n_i} + O\left(\frac{1}{{n_i}^3}\right)$$

So by replacing in $ln\Omega$ expression:

$$ln\Omega = \left[\left(N\, lnN - N + \frac{1}{2}ln(2\pi N)\right) - \sum_i \left(n_i\, ln\, n_i - n_i + \frac{1}{2}ln(2\pi n_i)\right)\right] + \left[\frac{1}{12N} - \sum_i \frac{1}{12n_i}\right] + \left[O\left(\frac{1}{N^3}\right) - O\left(\frac{1}{{n_i}^3}\right)\right]$$

Introducing the frequencies $P_i = \frac{n_i}{N}$:

-For linear terms:

$$\sum_i n_i\, ln\, n_i = \sum_i Np_i ln(Np_i) = N\, lnN \sum_i p_i + N \sum_i p_i\, ln\, p_i$$

Therefore with $-N + \sum_i n_i = 0\ because \sum_i n_i = N$:

$N\ lnN - \sum_i n_i\ ln\ n_i - n_i = -N \sum_i p_i\ ln\ p_i$ (A)

-For ½ terms:

$\frac{1}{2} ln(2\pi N) - \frac{1}{2} ln(2\pi n_i) = \frac{1}{2}[(m-1)lnN - \sum_i ln\,(2\pi n_i)]$ (B)

-For remainder terms because each n_i is at least dominated by $O(n/m)$ with *m* fixed:

$$\frac{1}{12N} - \sum_i \frac{1}{12n_i} = \frac{1}{12N}\left[1 - \sum_i \frac{N}{n_i}\right] = O(1/N)$$

Finally, assembling the pieces:

$$ln\Omega == -N \sum_i p_i\ ln\ p_i + \frac{1}{2}\left[(m-1)lnN - \sum_i ln\,(2\pi n_i)\right] + O(1/N)$$

Appendix 2: Two-state Boltzmann derivation of the adaptability function $A_\beta(\alpha)$

Consider the organizational state of an open system characterized by a scalar order parameter α ∈ [0, 1], where $\alpha = 0$ denotes maximal internal disorder and $\alpha = 1$ denotes perfect internal order. We model the system as occupying one of two macrostates, an *ordered* state *O* and a *disordered* state *D*, with effective free energies (log-likelihoods) assigned as:

$$\mathcal{F}_O(\alpha) = -\ln \alpha\,, \mathcal{F}_D(\alpha) = -\ln(1-\alpha)$$

Note on notation: throughout this appendix, $\mathcal{F}_O(\alpha)$ and $\mathcal{F}_D(\alpha)$ denote the effective free energies of the individual ordered and disordered macrostates respectively (not to be confused with the full order-parameter mapping $O_\beta(\alpha)$).

The rationale is that α directly measures the relative weight of boundary-driven (ordered) dynamics, so $\ln \alpha$ is the natural log-evidence for the ordered state, and symmetrically for $1 - \alpha$.

Partition function. At inverse temperature $\beta > 0$, the Boltzmann partition function over the two states is:

$$Z(\alpha, \beta) = e^{-\beta \mathcal{F}_O} + e^{-\beta \mathcal{F}_D} = \alpha^\beta + (1-\alpha)^\beta$$

and the probability of occupying the ordered state is:

$$O_\beta(\alpha) = \frac{\alpha^\beta}{Z(\alpha, \beta)} = \frac{\alpha^\beta}{\alpha^\beta + (1-\alpha)^\beta}$$

This is equivalent to a logistic sigmoid in log-odds space:

$$O_\beta(\alpha) = \sigma(\beta \cdot \mathrm{logit}(\alpha)), \mathrm{logit}(\alpha) = \ln \frac{\alpha}{1-\alpha}$$

Susceptibility (adaptability). The thermodynamic susceptibility, the sensitivity of the ordered-state probability to changes in α is:

$$A_\beta(\alpha) = \frac{1}{\beta} \frac{dO_\beta}{d\alpha} = \frac{\alpha^{\beta-1}(1-\alpha)^{\beta-1}}{(\alpha^\beta + (1-\alpha)^\beta)^2}$$

Maximum and viability window. By symmetry, A_β is maximized at $\alpha^* = 0.5$, where A_β $(0.5) = 1$ after normalization. The vitality window $A_\beta\ (\alpha) \geq \theta$ (with $\theta = 0.9$ by default)

defines a symmetric interval $[\alpha_{min}, \alpha_{max}]$ around $\alpha^* = 0.5$. For $\beta = 2$, this yields $\alpha \in [0.406, 0.594]$; for $\beta = e$, the window narrows to $\alpha \in [0.435, 0.565]$.

Role of β as inverse temperature. The parameter β controls the stiffness of the order–disorder transition:

$\beta \to 0$ (high temperature): $O_\beta \to 1/2$ everywhere; the system is equally likely to be in either state and adaptability is uniformly distributed.

$\beta \to \infty$ (zero temperature): O_β becomes a Heaviside step function at $\alpha = 0.5$; adaptability collapses to a Dirac-like peak.

$\beta = 2$ (diffusion scaling): recovers a broad, ecologically meaningful vitality basin consistent with observed natural ecosystem distributions.

$\beta = e$ (multi-scale candidate): imposes a sharper thermodynamic criterion selecting only the most tightly organized systems.